Journal of Materials Chemistry B

ROYAL SOCIETY OF CHEMISTRY

PAPER

View Article Online
View Journal | View Issue

Check for updates

Cite this: J. Mater. Chem. B, 2024, 12, 10272

Photopatterning of conductive hydrogels which exhibit tissue-like properties†

Léo Sifringer,[a] Lina De Windt,[a] Stéphane Bernhard,[b] Giulia Amos,[a] Blandine Clément,[a] Jens Duru,[a] Mark W. Tibbitt[b] and Christina M. Tringides *[ac]

Received 12th April 2024,
Accepted 13th September 2024

DOI: 10.1039/d4tb00807c

rsc.li/materials-b

Hydrogels are three-dimensional, highly tunable material systems that can match the properties of extracellular matrices. In addition to being widely used to grow and modulate cell behavior, hydrogels can be made conductive to further modulate electrically active cells, such as neurons, and even incorporated into multielectrode arrays to interface with tissues. To enable conductive hydrogels, graphene flakes can be mechanically suspended into a hydrogel precursor. The conductivity of the hydrogel can be increased by increasing the weight percentage of graphene flakes in the precursor while maintaining the mechanical properties of the formed gel similar to the properties of neural tissue. By using a photocrosslinkable hydrogel matrix, such as gelatin methacrylate, with a photoabsorber, the conductive precursor solutions can be crosslinked into predefined complex patterns. Finally, the formulations can be used to support the growth of sensory neurons, derived from human induced pluripotent stem cells, for more than 7 weeks while the neurons remain viable. These scaffolds can be patterned into components of multielectrode arrays, to enable ultrasoft electrodes with tissue-matched properties for further interactions, both *in vitro* and *in vivo*, with the nervous systems.

1. Introduction

Implantable electrode arrays are often multi-material technologies composed of precisely patterned electrical components and encapsulated by insulating layers.[1–4] The electrical components are often composed of thin metal films that are highly conductive and can record neural signals, but are ductile, brittle, and stiff.[5] In contrast, biological tissues are soft, dynamic, and viscoelastic materials.[6–8] The interface between implants and tissues is thus poor, and often leads to device failure or irreversible tissue damage.[9,10]

Recent efforts have focused on the replacement of metal films with conductive composites, made from either conductive polymers or conductive hydrogels. These soft conductive materials can be formed by various strategies, including (i) by polymerizing conductive polymers, such as poly(aniline)[11,12] or poly(3,4-ethylenedioxythiopene) polystyrene sulfonate (PEDOT:PSS),[13–15] into a soft matrix, or (ii) by mechanically trapping conductive nanoparticles or nanomaterials, such as carbon nanotubes, graphene flakes, or silver nanowires,[16,17] into a polymer network. Processing conductive polymers is often more reliable than the processing of conductive hydrogels as there is less liquid in the conductive polymers that could evaporate over time, the conductive polymers are more stable at higher temperatures, and the conductive polymers can undergo vacuum. However, these conductive polymer composites have mechanical properties that are more stiff[14,18] (200 kPa–2 MPa) than neural tissue (~0.5–2 kPa).[16,17]

Hydrogels are water-swollen polymer networks that can mimic the native extracellular matrix structure and composition of living tissues.[19–24] In particular, they can exhibit viscoelastic behavior with mechanical properties in similar ranges to those of living tissues.[7,25] Often, hydrogels have been used to provide mechanical support to cells in culture; after defining a material with a specific mechanical microenvironment that mimics that of the native *in vivo* environment, cells can be cultured either on top or inside the materials.[26–30] However, introducing additional functionalities, such as conductivity, in the hydrogel matrix would broaden the range of possible applications for electrical recording or stimulation of neural cells or tissues.[31] By applying exogenous electrical stimulation throughout the material, the conductive hydrogel can be used to further modulate neural cell networks. Alternatively, these conductive formulations can be used as implantable electrodes that can record neural signals without compressing or damaging the underlying tissue.

[a] Laboratory of Biosensors and Bioelectronics, Institute for Biomedical Engineering, ETH Zürich, Switzerland. E-mail: ct81@rice.edu
[b] Macromolecular Engineering Laboratory, Department of Mechanical and Process Engineering, ETH Zürich, Zurich, Switzerland
[c] Department of Materials Science and Nanoengineering, Rice University, Houston, TX, USA

† Electronic supplementary information (ESI) available. See DOI: https://doi.org/10.1039/d4tb00807c

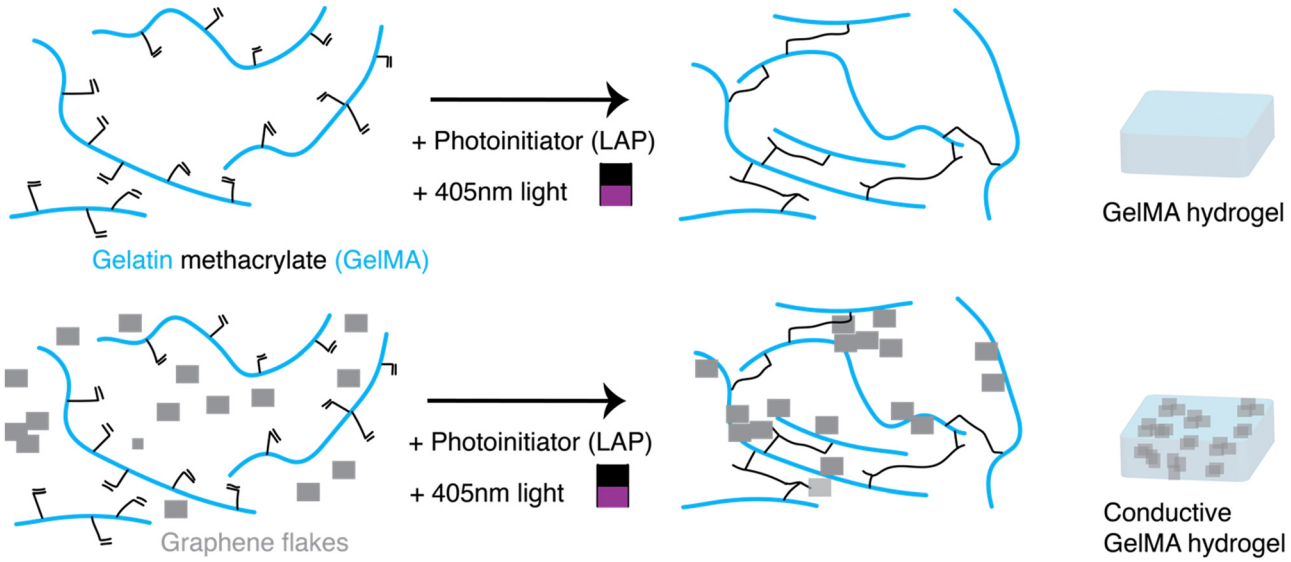

Fig. 1 A photocrosslinkable conductive hydrogel platform. (Top) When a gelatin methacrylate (GelMA) precursor, with a gelatin backbone (light blue) and methacrylate side-groups (black) is mixed with a photoinitiator, lithium phenyl 2,4,6 trimethyl (LAP), and exposed to 405 nm light (black/purple rectangle), the solution forms a hydrogel. (Bottom) By incorporating conductive fillers, such as graphene flakes (gray) into the mixture, the conductive material is mechanically trapped between the GelMA polymer chains and forms a conductive hydrogel.

Often, these conductive hydrogels are cast in tissue-culture plates or processed in various shapes through 3D-printed molds that have feature sizes in the range of hundreds of μms. However, both these methods show limited resolution in the resulting pattern. The ability to pattern these conductive formulations with finer resolution would facilitate their integration of these materials into implantable electrode arrays.[32,33] Doing so would introduce a conductive materials toolbox that can match the mechanical properties of living tissues.[24] To overcome these limitations, various photopolymerizable hydrogel formulations have been described over the last decade that can be crosslinked with LED lamps, digital light processing, and photolithography.[34–42] While photolithography can be used to achieve fine features (<1 μm), it requires photoresists, often reducing the biocompatibility of the material. Further, the techniques described above can require extended periods of time for sample preparation, alignment or calibration of the system, and likely lead to drying of the hydrogel, thus modifying its mechanical properties and possibly leading to a loss in tissue-like properties.

Here, we describe a simple method to produce biocompatible conductive hydrogels with mechanical properties that match that of neural tissues (<1 kPa), in a short period of time (< 2 minutes), and with a pattern precision of ~10 μm. By combining a photopolymerizable hydrogel matrix, such as gelatin methacrylate (GelMA), with conductive additives, such as graphene flakes (GF), conductive hydrogels with tunable mechanical and electrical properties could be fabricated through photopolymerization (Fig. 1). Crosslinking of the polymer network could be achieved through a LED lamp. To further increase the resolution of the patterning, a photoabsorber (tartrazine) was incorporated in the hydrogel formulation enabling the use of a confocal microscope laser (λ = 405 nm) as the light source for higher resolution of crosslinking. Recovery of the patterned hydrogel was achieved through simple washing steps of the non-crosslinked precursor solution. Finally, human-derived sensory neurons were added either into the precursor solution to be encapsulated inside the hydrogels, or on top of photopatterned hydrogel formulations. Both methods supported cell growth for more than 6 weeks *in vitro*. In addition to sustained cell viability, the sensory neurons interacted with the GF and formed networks around these conductive additives.

2. Experimental section

2.1 Preparation of gelatin methacrylate (GelMA) precursor mixtures

Gelatin methacryloyl, GelMA, (Sigma Aldrich, 900496) with gel strength 300 g Bloom and an 80% degree of substitution of methacrylated groups was used. Approximately 100–200 mg of the dried powder was weighed out into a 5 mL Eppendorf tube, and then sterile phosphate buffered saline (PBS; Merck, 806552) was added to prepare a 13% weight/volume (w/v) stock solution of GelMA. The Eppendorf was placed in a dry-bead bath at 37 °C for 30–45 minutes, and the tube was gently rocked every 10–15 minutes to facilitate the dissolution in PBS. After formation of a uniform solution, the formulation was filtered with a Millex PVDF syringe filter, 0.45 μm pore size (Millipore, SLHVR334B), into an autoclaved 1.6 mL Eppendorf tube. The formulation was stored in a 4 °C fridge until ready for use, at which point the tube was moved to the dry bath (37 °C) to allow the GelMA to warm for easier handling.

Precursor solutions were prepared by mixing GelMA stock solution, PBS, laminin (Roche, L2020), and a photoinitiator, lithium phenyl 2,4,6 trimethyl (LAP; at a final concentration of

0.05% w/v). While the ratio of GelMA and PBS was varied to change the final w/v% of the GelMA hydrogels, the total volume of the precursor solution was kept to 50 μL, and the amount of laminin (2.75 μL) and LAP (10 μL) was kept constant across all the formulations.

2.2 Preparation of conductive GelMA precursor mixtures

To prepare conductive hydrogel formulations, the same steps as in 2.1 were followed, but rather than adding only PBS to the precursor formulation, a hydrophilic suspension of graphene flakes, (GF; E-Graphene, Sixonia-Tech, Dresden Germany; flake concentration of 2.4 mg mL^{-1} in water) was instead added. The total volume of the precursor solution was kept to 50 μL, and the GF were mixed with a P1000 pipette before added to the solution to ensure uniformity of the suspension.

2.3 Preparation of bulk bare and bulk conductive GelMA hydrogels

Once the precursor formulations were prepared, a droplet of the mixture was added to a glass slide pretreated with Sigmacote (Sigma Aldrich, SL2) to minimize sticking of the formed hydrogels to the glass slide. After placing two poly(methyl methacrylate) PMMA spacers of 500 μm thickness, cut 1 mm × 4 mm with a Trotec Laser Cutter, on either side of the glass slide, a second Sigmacote-treated glass slide was placed on top of the droplet, to ensure (i) uniform thickness of the hydrogel, and (ii) to minimize evaporation of the small volume. A 405 nm LED lamp (Thorlabs), set to a power intensity of 20 mW cm^{-2}, was placed on a stand directly above the glass slides. The formulations were exposed to the light for a duration of 100 s. After illumination, the top slide was carefully removed with a pair of flat-tip forceps. The forceps were then dipped into sterile PBS and used to scoop the crosslinked hydrogel from the bottom glass slide into a sterile Petri dish filled with sterile PBS. To prevent the LAP from becoming inactive due to exposure to light, the precursor solution was covered in aluminum, and a new batch of precursor was prepared every 45 minutes. All of these steps, including the crosslinking with the LED lamp, were done under a biosafety cabinet to ensure sterility of the formulations.

2.4 Mechanical characterization of bulk conductive hydrogels

Bulk mechanical characterization of the bare and conductive GelMA hydrogels was done with a shear rheometer (MCR 502; Anton Paar) with a Peltier stage set to 37 °C and an 8 mm diameter parallel plate geometry. To avoiding loading history effects, the samples underwent an oscillatory preconditioning interval (ω = 1 rad s^{-1}, γ = 0.1%, t = 300 s). Dynamic oscillatory strain amplitude sweeps were performed at constant frequency, was done across each sample which had been trimmed to fill the space between the geometry and the plate. A gap size of 0.35–0.4 mm was used for all rheological measurements. A hydrated Kimwipe was placed under the plate to provide a humid environment.

2.5 Electrical characterization of conductive hydrogels

For the electrical characterization of the conductive hydrogels, molds that were 4 mm × 14 mm × 0.7 mm (width (w) × length (l) × thickness (t)) were 3D printed (Sonic Mini 4k, Phrozen) as a negative master mold. Ecoflex (Ecoflex 00-30, Smooth-On) was prepared and cast into the negative master molds and cured at 65 °C overnight. The Ecoflex molds were then carefully peeled off and plasma-activated (Tergeo, PIE Scientific) immediately before casting of the gel using the following parameters:[43] 1 min, 100 W, 10 sccm O_2.

All the components for the conductive hydrogels were prepared and mixed to prepare a uniform solution (100 μL) to fill the mold. Each filled structure was crosslinked for 2 minutes, and immediately filled with PBS after to prevent dehydration of the hydrogels. To prevent dehydration during the crosslinking step(s), a hydrated Kimwipe was placed inside a Petri dish which contained the Ecoflex mold, and the dish was covered with a transparent lid.

To measure the resistance of the gels, the Ecoflex molds containing the gels were taken out of the PBS, and the gels were probed immediately so that they would not dry. The resistance R was measured by a four-point probe method (Hioki IM3536 LCR meter). The conductivity (σ, S m^{-1}) was derived using the following formula:

$$\sigma = \frac{s}{twR}$$

where s is the probe spacing (2.54 mm).

2.6 Structural characterization of conductive hydrogels

To evaluate the structural properties of the conductive hydrogels, namely the distribution of the GF throughout the hydrogel matrix, scanning electron microscopy (SEM) was used. After making the conductive hydrogel formulations, as described above, the gels were dehydrated in increasing ethanol solutions. First, the hydrogels which were stored in PBS, were added to a 50–50 solution of PBS-ethanol (100%). After 30 minutes, the hydrogels were transferred to a 30–70 (PBS-ethanol) solution, followed by 20–80, 10–90 solutions. The hydrogels spent at least 30 minutes in each solution. Finally, they hydrogels were placed in 0–100 (pure ethanol solutions), over 2 iterations. After the final soak in the 100% ethanol solution, the hydrogels were left under a chemical hood overnight to allow the ethanol to dry.

Once the hydrogels were dried, they were mounted onto an SEM stub covered with carbon tape. One hydrogel remained intact for the imaging, while the other was broken to reveal the cross-section of the formulation. Prior to imaging, the samples were sputter-coated with AuPd to create a conductive layer (Leica EM ACE200, 1 min sputtering). The sample were then imaged in a Zeiss Ultra 55 plus scanning electron microscope using the following parameters: 5 kV, 4.2 mm WD, InLens SE detector.

2.7 Photopatterning conductive hydrogels

To create complex shapes, rather than just bulk hydrogels, illumination was performed using a defined region of interest (ROI) on an Olympus Fluoview 3000 confocal laser scanning microscope

(CLSM). When conductive hydrogel precursors, as described in 2.2, were crosslinked under the CLSM, the entire formulation that was exposed to the laser beam was crosslinked. This results in sequential circles, rather than a defined pattern. In order to maintain the resolution of the features, and to avoid crosslinking the surrounding precursor solution that was not in the ROI, tartrazine (Sigma Aldrich, SKU-03322) was added to the precursor formulation. Though a food dye, tartrazine also acts as a photoabsorber, and can facilitate the desired patterning of a particular structure.[36]

25 mg of tartrazine was dissolved into 10 mL of sterile PBS, and the solution was thoroughly mixed. The tartrazine was added to the hydrogel precursor solution at a 1 : 5000 dilution, so that the total w/v% of the tartrazine was 0.1%. The amount of GF and PBS were adjusted to keep the total volume of the formulation consistent. To confirm gelation, 5 μL of formulation was first tested as described in Section 2.3, to ensure crosslinking.

Once the tartrazine containing conductive hydrogel precursor was prepared, the solution was uniformly mixed and 10 μL was placed on a clean glass slide. After placing two PMMA spacers of 500 μm thickness, cut 1 mm × 4 mm with a Trotec laser cutter, on either side of the glass slide to ensure a uniform thickness of the hydrogel and minimize the evaporation of the precursor formulation, the slide was loaded into the stage of the CLSM. Another clean glass slide was placed on top of the conductive gel precursor, and a 647 nm laser was used to find and focus on the droplet. To create 'before', 'during' and 'after' images of the droplet, without pre-crosslinking the gel, images were acquired using the 647 nm laser line at 10× or 20× magnfication.

After establishing the focus and field of view, a polygon ROI was used to draw the desired patterns at each location. Next, a 405 nm laser line was set from 1 to 80% power intensity, with exposure from 30 to 300 s. Upon crosslinking, images of the formed hydrogel were recorded as previously mentioned using a 647 nm laser. The patterning procedure was repeated by moving the objective to a new location and defining a new ROI. Once all the regions of a given precursor formulation were patterned, the top glass slide was carefully removed. The bottom glass slide, which had the crosslinked hydrogels and remaining unreacted precursor solution, was placed in a larger Petri dish and filled with sterile PBS. The Petri dish was placed on a shaker (Fisher Scientific 88861023 Microplate Shaker) overnight at 55 rpm to wash the unreacted precursor solution away. The next day, the solution was removed, and the glass slides with crosslinked patterned hydrogels were placed under a bright field microscope (Leica DM750), and imaged.

2.8 Assessment of conductive hydrogels for cell culture

Human-derived sensory neurons, 'hDRG', (Real DRG Female Line#1, Catalog #1020F-1M) from Anatomic Incorporated (Minneapolis Minnesota, USA) were purchased and stored in a liquid nitrogen cell tank until ready for use. The cells were thawed per manufacturer guidelines; briefly, by quickly removing the vial from the liquid nitrogen, placing it in an ice-filled Styrofoam box for transportation, and placing the vial into a water bath at 37 °C. Within 90 s, the ice from the vial had melted, and the cells were added to a sterile 15 mL Falcon tube, using a P1000 tip that had been pre-rinsed with the Senso-MM media (Anatomic, Catalog #1030). After centrifuging the cells at 100*g* for 3 min, the supernatant was removed and the pellet was resuspended in fresh Senso-MM media.

The cells were then assembled into spheroids. To form spheroids of equal size (200 cells per spheroid), a 24-well Aggrewell 800 plate (Stemcell Technologies) was used according to manufacturer guidelines. Briefly, 1 mL of Anti-Adherence Rinsing Solution (Stemcell Technologies, CAT #07010) was placed in each well to be used, and centrifuged for 5 min at 1400*g*. After confirmation of the absence of bubbles in the microwells, the solution was removed, and fresh media was added. Next, the thawed cells were added to each well at the appropriate concentration to form spheroids of the desired size. The plate was then centrifuged for 3 min at 100*g*, and carefully placed in an incubator at 37 °C and 5% CO_2 for at least 24 hours to allow for adequate formation of the spheroids.

The next day, a P200 micropipette was used to gently suspend the spheroids in a particular well. A 80 μL droplet of spheroids and media were placed on the lid of a small sterile Petri dish. A dissection microscope, placed under a Biosafety cabinet, was used to collect the desired number of spheroids and add them to the hydrogel precursor solution. The cell-laden precursor solution was exposed to the LED lamp, as described in Section 2.3, and the gels were transferred to an 18-well Ibidi dish filled with Senso-MM media, as per the manufacturer instructions, in which to be cultured over the remaining timepoints. After the recommended two weeks in which to culture the cells in the Senso-MM media, the neurons were cultured in a maintenance media of neurobasal medium, 5% B27, 1% Glutamax, 1% sodium pyruvate, and 1% penicillin–streptomycin (all from ThermoFisher), in which the following were freshly added before each media change: BDNF, GDNF, NT-3 each at 20 ng mL^{-1}, NGF at 50 ng mL^{-1}, forskolin at 10 μM.

Alternatively, the hydrogels could first be prepared with tartrazine as described in Section 2.6 and crosslinked with the LED lamp to ensure sterility of the formulations. The gels could either be crosslinked as bulk hydrogels (through exposure to the lamp directly) or patterned by placing a defined pattern on the outermost portion of the top-glass slide. Once the hydrogels were crosslinked, they were transferred to a tissue culture dish and submerged with media. The formed spheroids could then be added on top of the hydrogels.

2.9 Evaluation of cell viability and growth through conductive hydrogels

To evaluate the hDRG viability over DIV 1–8, the desired well was incubated with Calcein AM dye (Invitrogen, 65-0853-39). The dye was added to the cell media at a 1 : 1000 ratio. After 20 minutes, the solution was replaced with fresh, warmed, media and the samples were imaged under the Olympus Fluoview 3000 CLSM, with its stage top incubator set to 37 °C and 5% CO^2. A 561 nm laser line was used to excite the fluorophore, and the images were acquired using a 10× and

20× objective. After the imaging session, the media was replaced once more with fresh media. For later time points, a fresh (previously unstained) hydrogel sample was used as the Calcein AM dye seemed to induce cell death after 24 h of incubation, despite frequent washings with fresh media to remove residual traces of the dye.

A Leica brightfield microscope (Leica DM750) was used to image the cell-laden hydrogels over various time points. The media was replaced, following manufacturer guidelines, twice a week by removing half of the current media and adding the same volume of fresh, warmed media.

2.10 Immunohistochemistry (IHC) of sensory neurons in conductive hydrogels

The hDRG-laden conductive hydrogels were fixed at DIV 45 by removing all of the media, rinsing the gels once with sterile

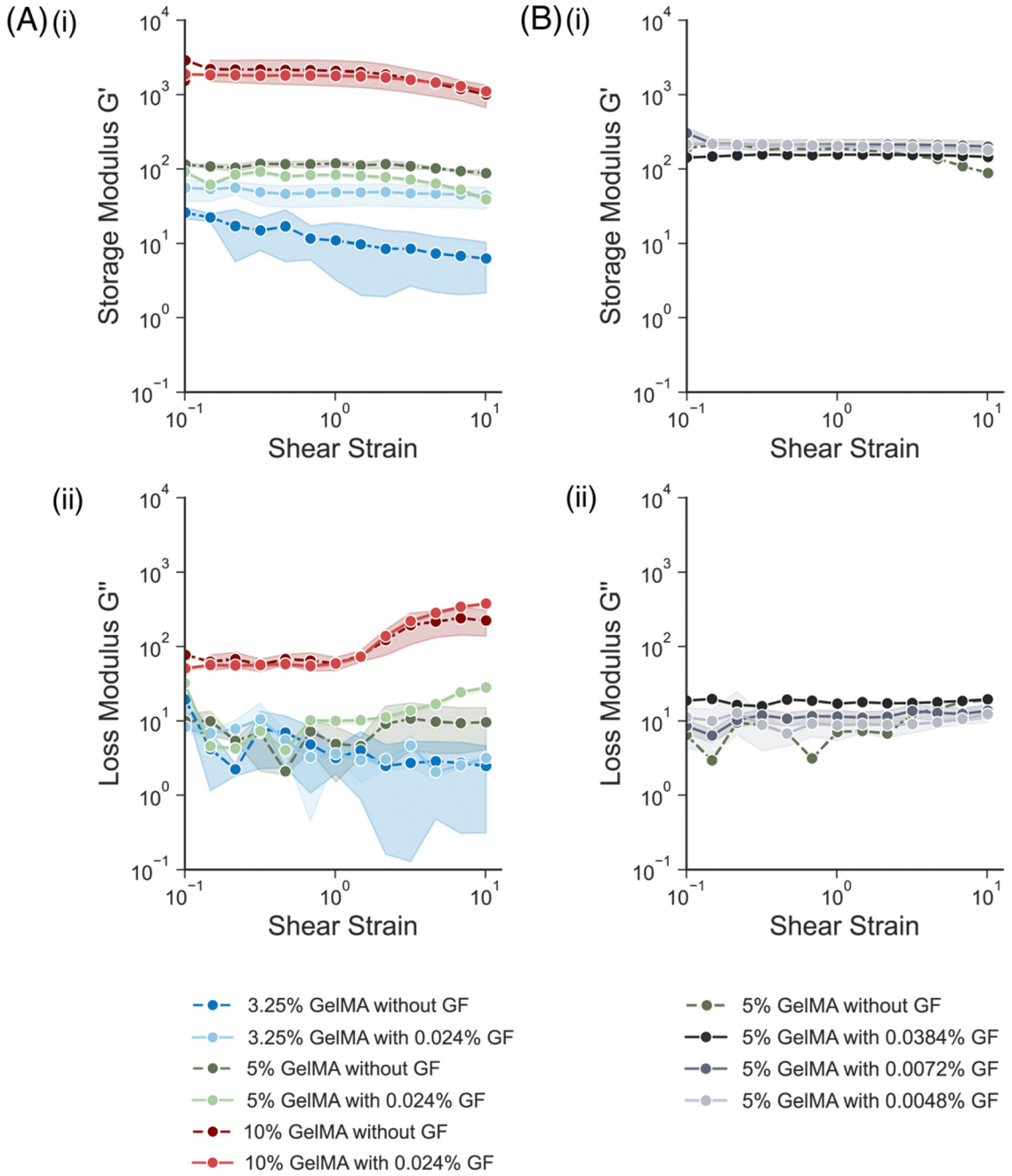

Fig. 2 Bulk mechanical characterization of different w/v% GelMA conductive hydrogels, and of different w/v% GF in 5% w/v GelMA hydrogels, as a function of strain. (A) (i) Storage modulus, G' and (ii) loss modulus, G'', of different w/v% GelMA hydrogels, with and without graphene flakes (GF), across a strain sweep. An n = 3 of each gel formulation was measured, and the mean and standard deviation are plotted. (B) (i) Storage modulus, G', and (ii) loss modulus, G'', of different w/v% GF conductive hydrogels, all in a matrix of 5% w/v GelMA. The 0% GF was n = 1, all other samples were n = 2–3. Mean and standard deviation are plotted.

PBS, and then adding enough 4% paraformaldehyde, (PFA; ThermoFisher, Catalog number 043368.9M) solution, diluted in PBS, to submerge the gels. After 15 min, the PFA solution was removed and the gels were rinsed 3 times with PBS. The samples were stored in PBS until further use.

To permeabilize the cells, 0.1% Triton-X (ThermoScientific, PI85111) dissolved in PBS was added to each well and kept for 7 min. Next, six 10 min washes with PBS were done to each gel. Then, primary antibodies were added at a 1:500 ratio to a blocking buffer solution (5% goat serum in PBS). The primary antibodies (SMI312 (mouse), Biolegend Catalog #827904; peripherin (rabbit), Abcam ab246502) were left overnight, on a shaker. The next day, the primary solution was removed and the gels were washed with fresh PBS (at least six washes, spread out over a minimum of 5 h). When the washing steps were complete, the secondary antibodies (AlexaFluor Anti-Mouse 555, AlexaFluor Anti-Rabbit 488) were added at a 1:500 to blocking buffer, placed to cover each gel, and then covered by aluminum foil. The samples were left, protected from light, on the shaker overnight. On the third day, six washes, each of at least 10 min, were done with PBS, followed by the addition of Hoechst 33342 (ThermoScientific, Catalog number 62249) at a 1:500 ratio to blocking buffer. The Hoechst was incubated, covered by aluminum foil, at room temperature for 30 min, after which 2 more washes with PBS were done. The stained gels were carefully transferred to a glass slide, covered with a drop of Prolong Gold Antifade Mountant (Invitrogen, Catalog number P36930), and imaged with the CLSM.

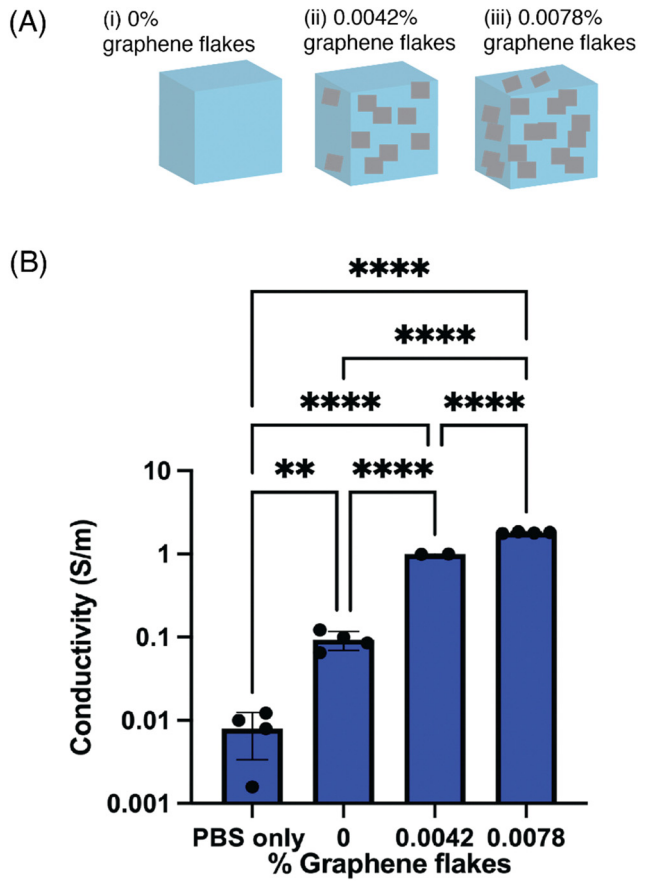

Fig. 3 Electrical characterization of conductive hydrogels in a 5% w/v GelMA with increasing amounts of w/v% GF. (A) Schematics representing the relative amounts of graphene flakes across the formulations tested: (i) 0% w/v GF, (ii) 0.0042% w/v GF, (iii) 0.0078% w/v GF. (B) Plot showing the conductivity of different conductive hydrogel formulations, as a function of the w/v% GF added into the gel. N = 2–3 samples were measured for each condition, each from a different batch of gel precursor, and mean and standard deviation are plotted. Numerical data are presented as mean ± s.d. (one-way analysis of variance (ANOVA) and Tukey's honestly significant difference (HSD) *post hoc* test: $^{****}P < 0.0001$, $0.001 < {}^{**}P < 0.01$).

3. Results and discussion

3.1 Fabricating conductive GelMA hydrogels and measuring the mechanical properties

Before patterning the conductive hydrogels, the mechanical and electrical properties of the composites were characterized. First, the mechanical properties of gelatin methacrylate (GelMA) hydrogels were assessed. GelMA solutions at different weight/volume percentages (w/v%), 3.25%, 5% and 10% w/v, were prepared and crosslinked using an LED lamp (λ = 405 nm). The mechanical properties of the resulting bulk

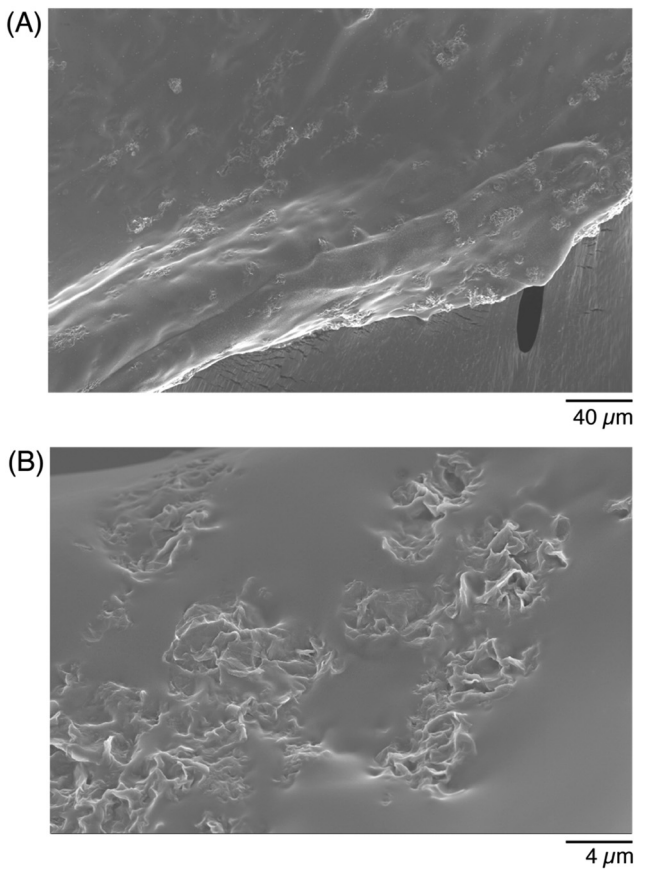

Fig. 4 Structural characterization of conductive hydrogels using scanning electron microscopy (SEM). (A) Photomicrograph of a 5% w/v GelMA hydrogel with 0.0042% GF, to show a larger portion of the gel, and (B) a zoomed-in portion of the GF embedded in the GelMA hydrogel matrix.

hydrogels were assessed using a rheometer. Both the storage modulus (G') (Fig. 2A(i)) and loss modulus (G'') (Fig. 2A(ii)) were determined from strain amplitude sweep measurements. As the w/v% of the GelMA increased, the modulus increased from ~25 Pa to ~2.5 kPa. Next, GelMA solutions at the same w/v% were prepared, adding 0.024 w/v% of graphene flakes (GF) to each precursor solution. For the formulations made from 5% w/v and 10% w/v GelMA, the addition of GF showed little effect on the mechanical properties of the gels. Similar trends were observed in other conductive hydrogels that incorporated nanomaterial additives into the hydrogel matrix.[17,22] While the GF formulation is hydrophilic and quite uniform in distribution, any aggregation of the flakes could lead to changes in the interactions of the polymer chains. In contrast, for the formulation with 3.25% w/v GelMA, the addition of GFs increased the G' by almost double (from ~25 Pa to ~44 Pa at 0.1% strain). This could be because the GelMA itself is so soft, at just 10 s of Pa, whereas the higher w/v% are more stiff (~100 s or 1000 s of Pa), and thus the GF contribute more to the mechanics of the softest matrix. Interestingly, the variability (error bars) in G' over the strain sweep was less for the hydrogels with GF than with the bare GelMA. Since GF offer some structural support to the gel, their presence could have added to the integrity of the sample and thus resulted in more consistent measurements.

Conductive hydrogels, all with a 5% w/v GelMA, with varying concentrations of GF (0.0048%, 0.0072%, 0.0384% w/v GF) were also fabricated and compared (Fig. 2B). Varying the w/v% of GF had no effect on the storage modulus measured, as all the formulations had a G' between 180 Pa and 260 Pa at 0.1% strain (Fig. 2B(i)). The loss modulus, G'', for the formulations with higher% w/v GF was slightly higher (Fig. 2B(ii)), especially compared to the bare GelMA.

Overall, the addition of GFs into the GelMA precursor formulation did not seem to have a significant impact on the mechanical properties of the resulting mechanical properties. All formulations remained in a range similar to the mechanical properties of neural tissue.

3.2 Evaluating the electrical properties of the conductive hydrogels

Next, the electrical properties of conductive hydrogel formulations with different amounts of GF were compared (Fig. 3). The sheet resistance of bare 5% w/v GelMA was first measured, and then the sheet resistance of three conductive formulations (0.0042%, 0.0078%, 0.0384% w/v GF) (Fig. 3A). As the w/v% of GF increased, the sheet resistance tended to drop and the corresponding conductivity increased (Fig. 3B). For the formulations with the highest amount of GF (0.0384% w/v GF), the samples dehydrated more quickly which affected the formation

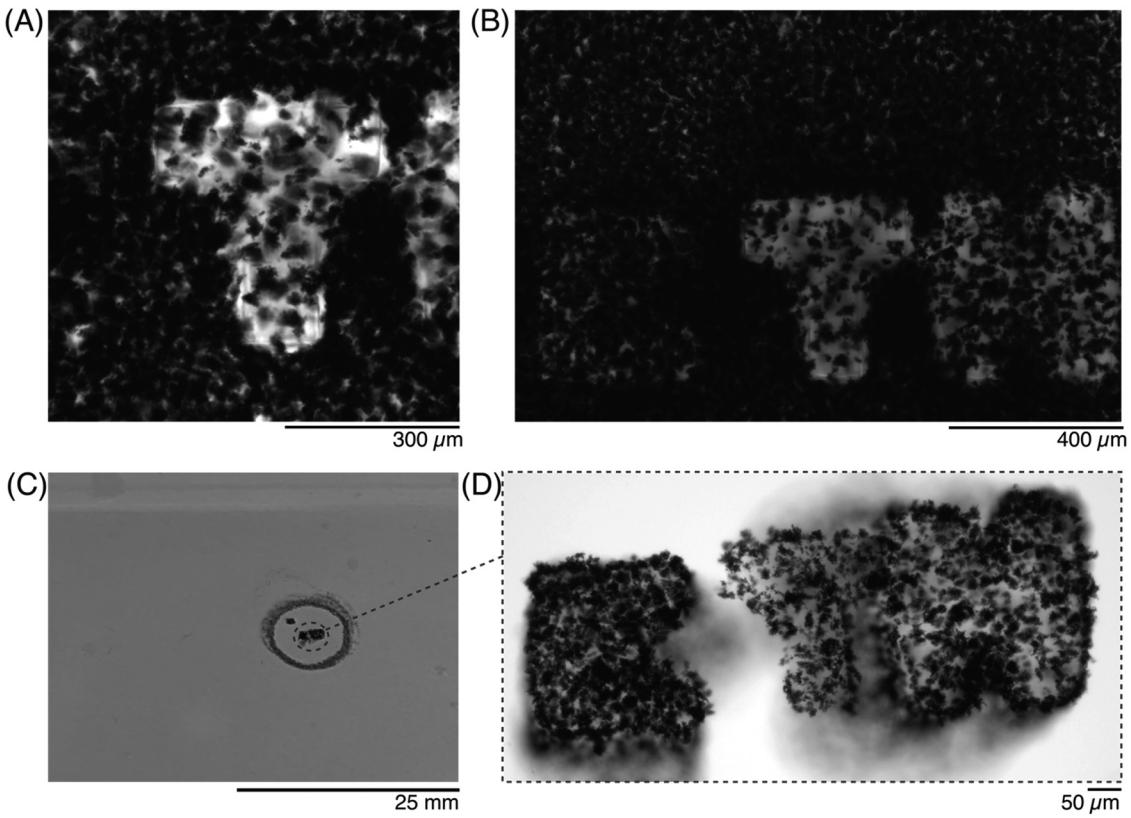

Fig. 5 Photopatterning of conductive hydrogels with a confocal laser scanning microscope (CLSM), showing the workflow of the patterning process. (A) Photomicrograph of one ROI, zoomed-in, to show the crosslinked gel. (B) Photomicrograph of the patterned ROIs, in the 647 nm channel. (C) Photograph of the washed hydrogel, with the pattern semi-visible by eye, and (D) photomicrograph of the pattern after washing.

of a hydrogel. When the samples were then rehydrated with PBS, there were broken gel fragments that were released from the mold, and thus a considerable amount of GF that broke off from the gel fragments. These discontinuous gels were measured, but not plotted, as the sample geometry and repeatability was difficult to determine. In the formulations measured and plotted, however, the variability between gels was quite low, as indicated by the standard deviation. Further, two different mold geometries were used to calculate the sheet resistance and conductivity, which found no differences in the electrical properties.

3.3 Evaluating the structural properties of the conductive hydrogels

The last materials characterization was evaluating the structural composition of the conductive hydrogels. A formulation of 0.0042% GF was added into a 5% w/v GelMA hydrogel matrix, and crosslinked. The conductive hydrogel was then prepared for analysis under scanning electron microscopy (SEM), to show the distribution of the flakes into the hydrogel matrix. Because the GF were purchased as an aqueous dispersion, they distributed throughout the matrix rather than formed a large aggregate (Fig. 4A). The smooth portion of the image was the GelMA portion, while the small rougher regions represent the GF. Flakes formed small clusters that were able to distribute throughout the entire matrix of the gel. When the cross-section of the gel was imaged, to visualize how the additives were able to span the thickness of the gel, they were found to also distribute throughout the gel (Fig. 4B). At this higher magnification, the flake morphology was better visible. Although the GF distribution was quite uniform in the entire volume of the hydrogel, it was visible that there was unlikely a percolating path at this concentration of additives. A higher concentration of flakes, or larger flakes that would better span the hydrogel, could help achieve percolation.

To evaluate the stability of the conductive hydrogels in PBS, the mass of the conductive hydrogels was measured after formation (before added into a PBS bath), after soaked for 30 minutes, and after soaked overnight in PBS. The relative change in mass was less than 5%, even after an overnight soak in PBS (Fig. S1, ESI†). As both the GelMA and the LAP were dissolved in PBS, the hydrogels were >94% PBS, which likely contributed to their stability and minimal swelling.

3.4 Photopatterning and processing the conductive hydrogel formulations

After characterizing the mechanical and electrical properties of the different formulations, one composition (0.0078% w/v GF)

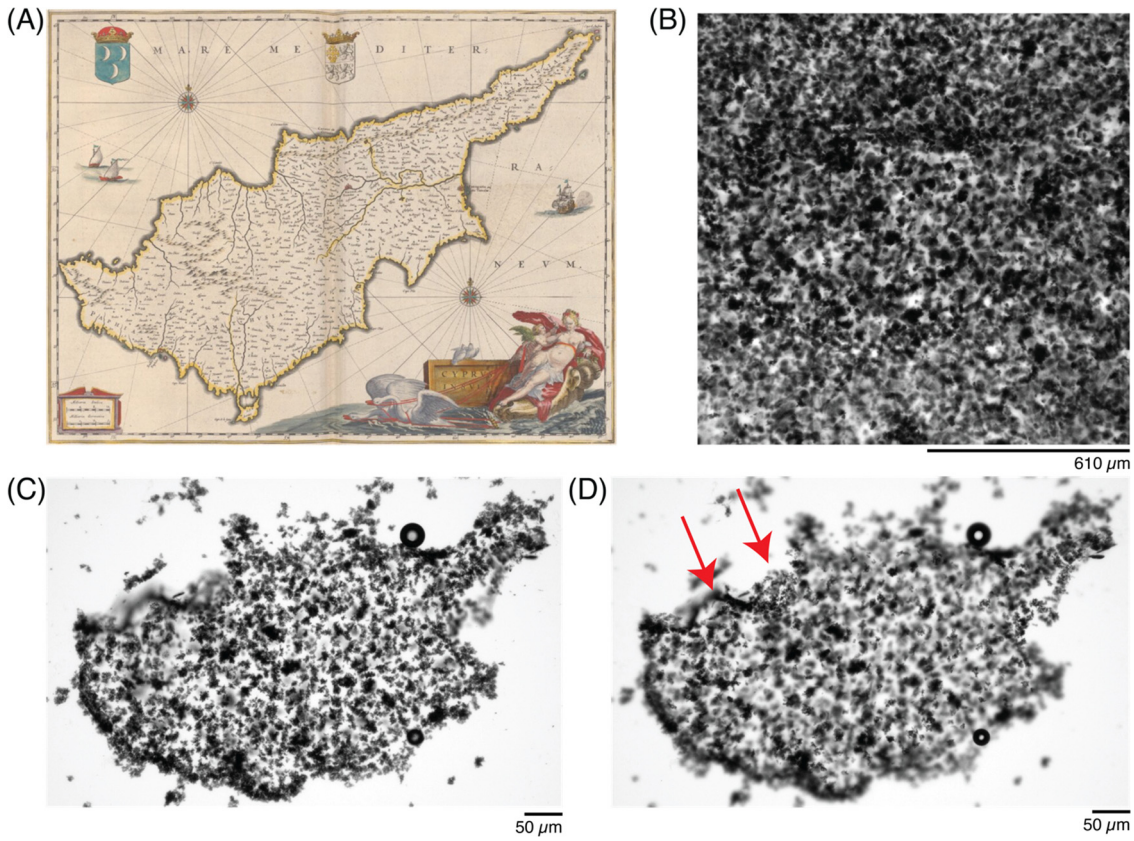

Fig. 6 Photopatterning complex shapes in conductive hydrogels. (A) Historic map of the Cyprus island from 1647–1664,[44] and a (B) photomicrograph of the patterned ROI, under transmitted light. (C) Photomicrograph of the patterned conductive hydrogel, washed, at one focal plane, and (D) photomicrograph of the same patterned conductive hydrogel, at a different focal plane (20 μm above in *z*-dimension), to show patterning in the *z*-dimension, highlighted by red arrows.

was selected to create complex hydrogel geometries and patterns. Initially, the precursor formulations, as described were exposed to an ROI. Despite the presence of the ROI, the entire precursor area exposed to the CLSM confocal laser was crosslinked and there were no distinguishable shapes. To allow for the patterning of the desired shape, a photoabsorber (tartrazine) was incorporated into the precursor solution. The presence of the photoabsorber allowed the precursors to instead adopt the desired shapes. In order to minimize the amount of photoabsorber added, various precursor formulations were exposed to a circle ROI and a square ROI, at different regions in the solution. The amount of tartrazine was increased for each formulation, in increments of 0.5% w/v, and stopped once the desired shapes were crosslinked. For the following formulations and experiments, a precursor solution with a final tartrazine concentration of 1.5% w/v solution was used.

To begin, more 'simple' shapes with 90° angles were selected as ROIs and the patterns were exposed to the underlying hydrogel formulation. A 'T' shape was exposed to the hydrogel, and the laser intensity and the duration of exposure was varied. Once the shape was patterned at different conditions throughout the precursor matrix, the samples were washed and assessed. The minimum time and power to produce reliably crosslinked hydrogels was 40% power and 90 s duration time, which was used for the remainder of the formulations.

Next, the letters 'E', 'T', and 'H', were patterned sequentially before washing away the unreacted precursor, using a 10× objective. The precursor solution was first imaged before any ROI was exposed (Fig. S2, ESI†), and then again after all 3 letters were patterned. After the exposure, the zoom was adjusted to focus on each letter, so that the crosslinked shape could be better appreciated (Fig. 5A). The crosslinked region was clearly distinct from the surrounding precursor solution, and as each subsequent ROI was patterned, the features of the previous letters were unchanged (Fig. 5B). Once the residual precursor was thoroughly washed and removed, it was visible that three separate hydrogels had been patterned (Fig. 5C) but morphologies were only visible once imaged (Fig. 5D). The GF that were trapped into the crosslinked hydrogels remained after the wash steps, despite the nonhomogeneous distribution of GF in the droplet (*e.g.*, higher amounts of GF for the 'E', lower GF amounts for the 'T' and 'H').

Once the letters were patterned, more complex ROIs were drawn. In particular, historic (Fig. 6) and modern-day (Fig. 7) maps of the country Cyprus were patterned into the precursor solutions. A small droplet of the solution was patterned to match the historic map (Fig. 6A[37]), and imaged after exposure

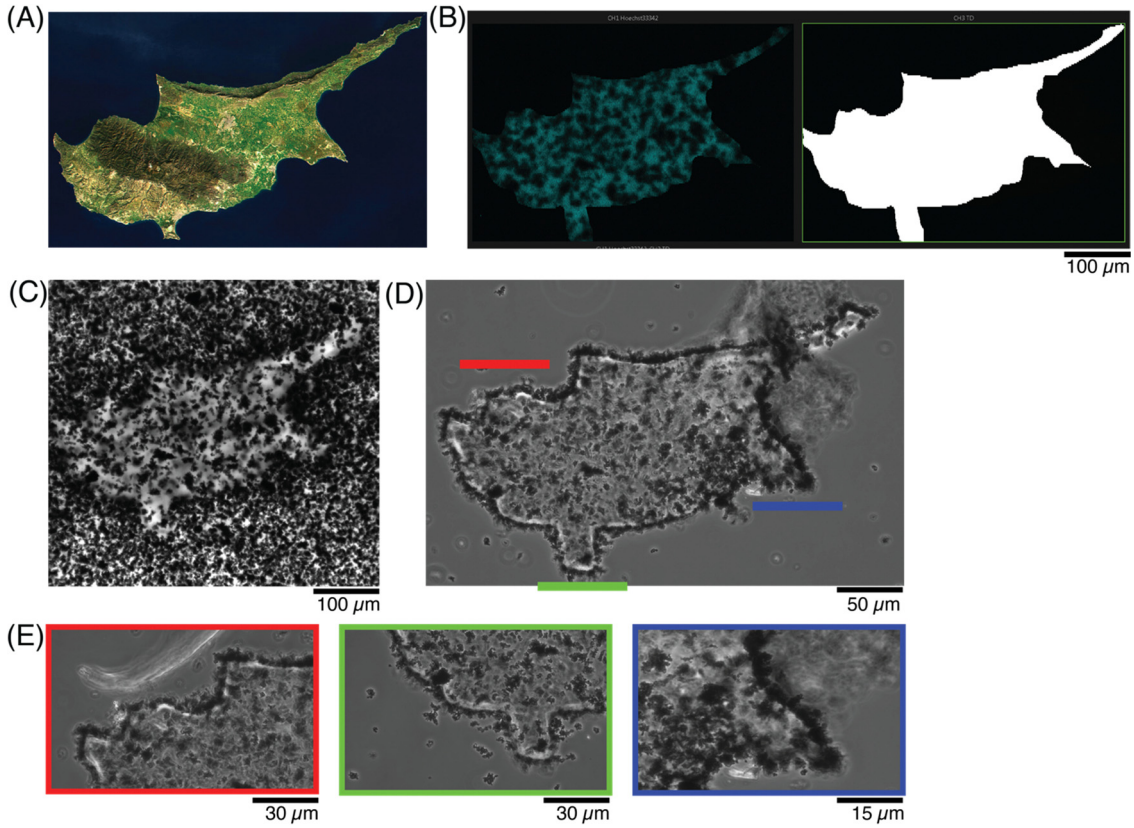

Fig. 7 Photopatterning shapes with higher resolution in conductive hydrogels. (A) Satellite image of the country,[45] as compared to the (B) scheme showing the new ROI, with more features and at smaller resolution size. (C) Photomicrograph of the patterned conductive hydrogel, before washing, and (D) after washing away the excess precursor to better visualize the pattern. (E) Photomicrographs at higher magnification of 3 regions of (C), to appreciate the resolution of the patterned ROI and its features.

to the ROI (Fig. 6B). By adjusting the *z*-height by 20 μm during the crosslinker duration, a 3D-profile could be patterned into the hydrogel to resemble the topography of the island (Fig. 6C and D).

A final demonstration at photopatterning was aimed to incorporate more features and identify the smallest dimensions that could be patterned. A modern-day map of Cyprus (Fig. 7A[38]) was drawn as a ROI (Fig. 7B), simultaneously showing the 405 nm laser line (left) and transmitted light channel (right). To achieve smaller features sizes, both a higher magnification objective (20×) and higher zoom (2.5×) were used to define a ROI, to match the country shape (Fig. 7C). Once the sample was washed, the features could be better appreciated and the shape was retained (Fig. 7D). In particular, when various locations were imaged under zoom, the pattern fidelity over a 20 μm region (Fig. 7E, red) and small indent of approximately 10 μm (Fig. 7E, green) were differentiated, although a small ∼5 μm protrusion (Fig. 7E, blue) was more difficult to resolve.

3.5 Incorporation of human sensory neurons into the conductive hydrogels

Human-derived sensory neurons, or 'hDRG', were encapsulated as spheroids inside the 0.0078% w/v GF conductive hydrogels before patterning, or placed on top of the patterned hydrogels. First, the viability of the hDRGs inside the hydrogels was assessed at different time points with a live stain (Fig. 8). After the first 24 hours, or day-*in vitro* 1 (DIV 1), the hDRG spheroids had begun to form short neurites in all directions, with small branches of approximately 50–60 μm (Fig. 8A). The next batch of samples were stained and imaged at DIV 4, at which point the neurites had sprouted further (∼900 μm), and grew mainly in the focal plane of the spheroid, but also began to spread in the *z*-direction, as evident by the small neurites which start to appear 'discontinuous' as they travel through the gel and change their focal plane (Fig. 8B). A last timepoint was evaluated at DIV 8, at which the neurites had spread multiple millimeters, throughout a 150 μm thickness of the gel (Fig. 8C). As the neurites had grown substantially in the *z*-direction at this time point, the green-labeled neurites appear discontinuous or fragmented, as they were not able to be captured in a single plane. The imaging of *z*-stacks showed that the neurites grew at least 75 μm into the depth of the conductive hydrogel.

While the viability was not tracked with markers at further time points, hDRG spheroids were encapsulated and cultured in the conductive hydrogels for up to 45 days. The hDRG were imaged every other day to monitor their growth. Within 5 days, the cells had started to integrate the GF into the spheroids

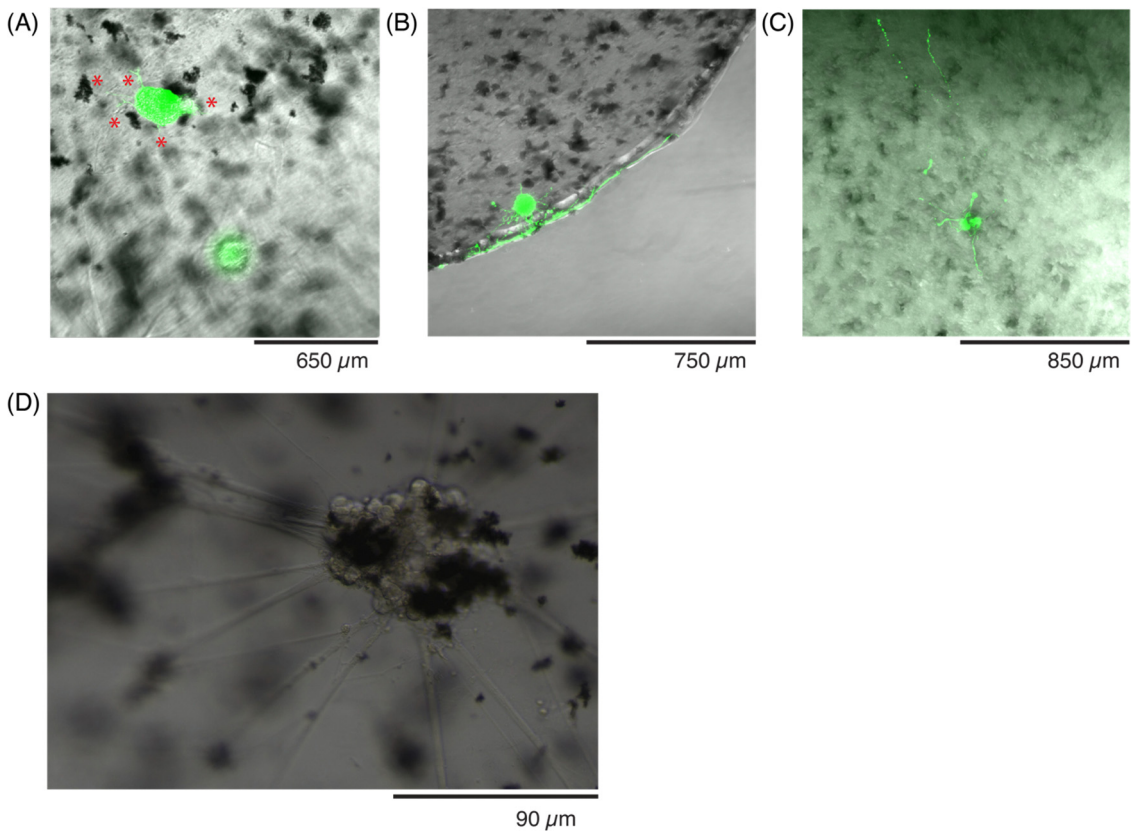

Fig. 8 Assessing the viability of sensory neurons in conductive hydrogels over 8 days. Photomicrographs of live human sensory neuron, hDRG, spheroids labeled in green (calcein) at (A) DIV 1, with initial neurite outgrowth indicated by red asterisks (*), (B) DIV 4, (C) a *z*-projection over a 150 μm stack taken at DIV 8, to assess cell viability and show the growth of the neurites at this timepoint. (D) Photomicrograph of the hDRG spheroids seeded on top of the conductive hydrogels at DIV 5.

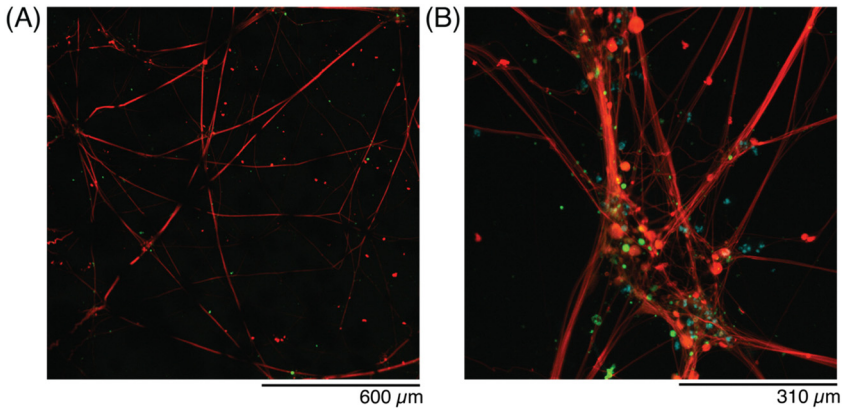

Fig. 9 Evaluating the morphology of sensory neurons at DIV45 in conductive hydrogels. Photomicrographs of sensory neurons seeded on top of the conductive hydrogels, at (A) 10× magnification and (B) 30× magnification. Red: SMI312 (axon marker), green: peripherin (DRG axon sub-type), cyan: Hoechst (nucleus).

(Fig. 8D), and the axons grew longer and in thicker bundles towards the direction of GF flakes in the hydrogel. The incorporation of GF did not lead to cell death, and the spheroids kept the GF throughout the entire experiment while remaining viable. By DIV 8, the axons had spread throughout the entire gel, and spanned the entire 150 μm thickness (Fig. 8C). The axons continued to grow close to the conductive additives, and it was observed that they often bridged different clusters of the GF. As neurons are electrically active cells, they could be influenced and guided by the enhanced conductivity of the material in regions with GF.[46] Additionally, another hypothesis could be that the GF have an increased surface area which could further modulate interactions with the neuronal cytoskeleton, and further promote growth throughout the hydrogel. As many of the hDRG cell bodies were in direct contact with GF, this could have an effect on the pathways for neurite outgrowth.

Finally, conductive hydrogels with hDRG seeded on top were fixed at DIV 45 and stained with antibodies to further evaluate the networks with immunohistochemistry (Fig. 9). The axons (red) spanned the entire volume of the gel, and traveled through nodes or bundles of GF (Fig. 9A). The presence of the flakes seemed to have no effect on the formation or extension of axons, as they had no change in thickness or angle when they exited a GF bundle. When the GF nodes were imaged under high magnification, the axon fibers were better visualized (Fig. 9B). In contrast, hDRG seeded on bare 5% w/v GelMA had randomly-oriented axons, which formed less fascicles, and less-dense bundles (Fig. S3, ESI†).

While the focus of this manuscript was on the patterning of the conductive hydrogel shape, in bulk, and allowing the neurites to grow out into the bulk hydrogel matrix, there are interesting considerations on if the hydrogel shape could be sub-patterned to promote neuronal growth. Past work has described how the presence of grooves could direct and influence the growth of neurites,[47–49] and other fabrication techniques can produce filaments that affect cell alignment.[50] Although the *z*-focus of the confocal laser could be adjusted to produce similar grooves, the neurites would be able to grow throughout the entire hydrogel (rather than just in the relief structure). To direct the growth of neurites into just the patterned relief, a hybrid material system, likely with an elastomeric container, would be needed to prevent outgrowth of the desired pattern.

4. Conclusions

We describe the fabrication and processing of conductive hydrogels which have tunable electrical and mechanical properties, while able to be patterned in a variety of shapes with improved resolution. Through defined ROIs on a confocal microscope, photopatterning of the conductive hydrogels to the 10 s μm scale was possible. By setting different ROIs across a *z*-stacks, the hydrogels can be patterned in all dimensions to create 'topographies'. Through modulation of the microscope and laser settings, and the relative amount of tartrazine, the feature-sizes can be explored. Finally, the patterned formulations are compatible with human sensory neurons (hDRG) and can support the growth and viability of the cells for multiple weeks. Altogether, the described system can be optimized both on the materials and cellular side, to create living materials for bioelectronics. While the hydrogel matrix reported in this study is gelatin-based, the approach is easily modifiable and compatible with any photocrosslinkable hydrogel. Further various conductive nanomaterial additives can be explored together, so that the combination of the multiple additives can modulate the final composite properties. By continuing to tune the electrical, mechanical, and structural properties of the hydrogels, the cell type(s) integrated into the material can be adapted as well, as well as the application of the composite material.

Author contributions

L. S. and C. M. T. designed the study and the experiments, with inputs from S. B. and initial feedback from J. D. C. M. T. and M. W. T. supervised the work. L. S., L. dW, G. A., B. C., C. M. T.

performed the experiments. L. S., G. A., and C. M. T. analyzed the data. C. M. T. wrote the initial draft of the manuscript, and all of the authors contributed to writing and editing of the manuscript.

Data availability

We are happy to share the data, including the raw experimental data upon reasonable request to the corresponding author.

Conflicts of interest

There are no conflicts of interest to declare.

Acknowledgements

We acknowledge Dr Céline Labouesse for synthesizing and sharing the LAP. The authors acknowledge financial support from ETH Zürich, and the ETH postdoctoral fellowship.

References

1 W. S. Konerding, U. P. Froriep, A. Kral and P. Baumhoff, New thin-film surface electrode array enables brain mapping with high spatial acuity in rodents, *Sci. Rep.*, 2018, **8**, 1–14.
2 W.-R. Lee, *et al.*, A convex-shaped, PDMS-parylene hybrid multichannel ECoG-electrode array. in 2017 39th Annual International Conference of the IEEE Engineering in Medicine and Biology Society (EMBC) 1093–1096 (IEEE, 2017), DOI: 10.1109/EMBC.2017.8037018.
3 A. Schander, *et al.*, A Flexible 202-Channel Epidural ECoG Array With PEDOT: PSS Coated Electrodes for Chronic Recording of the Visual Cortex, *IEEE Sens. J.*, 2019, **19**, 820–825.
4 E. Tolstosheeva, *et al.*, A Multi-Channel, Flex-Rigid ECoG Microelectrode Array for Visual Cortical Interfacing, *Sensors*, 2015, **15**, 832–854.
5 S. P. Lacour, G. Courtine and J. Guck, Materials and technologies for soft implantable neuroprostheses, *Nat. Rev. Mater.*, 2016, **1**, 16063.
6 C. M. Tringides and D. J. Mooney, Materials for Implantable Surface Electrode Arrays: Current Status and Future Directions, *Adv. Mater.*, 2022, **34**, 2107207.
7 O. Chaudhuri, J. Cooper-White, P. A. Janmey, D. J. Mooney and V. B. Shenoy, Effects of extracellular matrix viscoelasticity on cellular behaviour, *Nature*, 2020, **584**, 535–546.
8 O. Chaudhuri, *et al.*, Extracellular matrix stiffness and composition jointly regulate the induction of malignant phenotypes in mammary epithelium, *Nat. Mater.*, 2014, **13**, 970–978.
9 K. C. Spencer, *et al.*, Characterization of Mechanically Matched Hydrogel Coatings to Improve the Biocompatibility of Neural Implants, *Sci. Rep.*, 2017, **7**, 1952.
10 E. Otte, A. Vlachos and M. Asplund, Engineering strategies towards overcoming bleeding and glial scar formation around neural probes, *Cell Tissue Res.*, 2022, **387**, 461–477.
11 Z. L. Zhao, Z. L. Mo and Z. Y. Chen, Heterogeneous Preparation of Cellulose/Ag/Polyaniline Conductive Composite and its Electrical Property, *Appl. Mech. Mater.*, 2012, **182–183**, 254–258.
12 S. Jafarzadeh, P. M. Claesson, P.-E. Sundell, J. Pan and E. Thormann, Nanoscale Electrical and Mechanical Characteristics of Conductive Polyaniline Network in Polymer Composite Films, *ACS Appl. Mater. Interfaces*, 2014, **6**, 19168–19175.
13 M. Ganji, *et al.*, Development and Translation of PEDOT:PSS Microelectrodes for Intraoperative Monitoring, *Adv. Funct. Mater.*, 2018, **28**, 1700232.
14 B. Lu, *et al.*, Pure PEDOT:PSS hydrogels, *Nat. Commun.*, 2019, **10**, 1043.
15 D. Won, *et al.*, Digital selective transformation and patterning of highly conductive hydrogel bioelectronics by laser-induced phase separation, *Sci. Adv.*, 2022, **8**(23), DOI: 10.1126/sciadv.abo3209.
16 M. Carlotti and V. Mattoli, Functional Materials for Two-Photon Polymerization in Microfabrication, *Small*, 2019, **15**, e1902687.
17 N. He, *et al.*, Photoinhibiting via simultaneous photoabsorption and free-radical reaction for high-fidelity light-based bioprinting, *Nat. Commun.*, 2023, **14**, 1–15.
18 L. V. Kayser and D. J. Lipomi, Stretchable Conductive Polymers and Composites Based on PEDOT and PEDOT:PSS, *Adv. Mater.*, 2019, **31**, 1806133.
19 H. Geckil, F. Xu, X. Zhang, S. Moon and U. Demirci, Engineering hydrogels as extracellular matrix mimics, *Nanomedicine*, 2010, **5**, 469–484.
20 J. A. Rowley, G. Madlambayan and D. J. Mooney, Alginate hydrogels as synthetic extracellular matrix materials, *Biomaterials*, 1999, **20**, 45–53.
21 S. D. Dutta, D. K. Patel and K.-T. Lim, Functional cellulose-based hydrogels as extracellular matrices for tissue engineering, *J. Biol. Eng.*, 2019, **13**, 55.
22 R. S. Stowers, Advances in Extracellular Matrix-Mimetic Hydrogels to Guide Stem Cell Fate, *Cells Tissues Organs*, 2021, 1–18, DOI: 10.1159/000514851.
23 M. W. Tibbitt and K. S. Anseth, Hydrogels as extracellular matrix mimics for 3D cell culture, *Biotechnol. Bioeng.*, 2009, **103**, 655–663.
24 D. W. Nelson and R. J. Gilbert, Extracellular Matrix-Mimetic Hydrogels for Treating Neural Tissue Injury: A Focus on Fibrin, Hyaluronic Acid, and Elastin-Like Polypeptide Hydrogels, *Adv. Healthcare Mater.*, 2021, **10**, e2101329.
25 C. M. Tringides, *et al.*, Tunable Conductive Hydrogel Scaffolds for Neural Cell Differentiation, *Adv. Healthcare Mater.*, 2022, 2202221, DOI: 10.1002/adhm.202202221.
26 I. Levental, P. C. Georges and P. A. Janmey, Soft biological materials and their impact on cell function, *Soft Matter.*, 2007, **3**, 299–306.
27 P. C. Georges, W. J. Miller, D. F. Meaney, E. S. Sawyer and P. A. Janmey, Matrices with Compliance Comparable to that

of Brain Tissue Select Neuronal over Glial Growth in Mixed Cortical Cultures, *Biophys. J.*, 2006, **90**, 3012–3018.
28 P. C. Georges and P. A. Janmey, Cell type-specific response to growth on soft materials, *J. Appl. Physiol.*, 2005, **98**, 1547–1553.
29 T. Yeung, *et al.*, Effects of substrate stiffness on cell morphology, cytoskeletal structure, and adhesion, *Cell Motil. Cytoskeleton*, 2005, **60**, 24–34.
30 C. F. Guimarães, L. Gasperini, A. P. Marques and R. L. Reis, The stiffness of living tissues and its implications for tissue engineering, *Nat. Rev. Mater.*, 2020, **5**, 351–370.
31 Y. Liang, L. Qiao, B. Qiao and B. Guo, Conductive hydrogels for tissue repair, *Chem. Sci.*, 2023, **14**, 3091–3116.
32 C. M. Tringides, *et al.*, Viscoelastic surface electrode arrays to interface with viscoelastic tissues, *Nat. Nanotechnol.*, 2021, **16**, 1019–1029.
33 S. Oribe, *et al.*, Hydrogel-Based Organic Subdural Electrode with High Conformability to Brain Surface, *Sci. Rep.*, 2019, **9**, 13379.
34 E. A. Guzzi, *et al.*, Hierarchical biomaterials via photopatterning-enhanced direct ink writing, *Biofabrication*, 2021, **13**, 044105.
35 B. Ko, *et al.*, Hydrogels for active photonics, *Microsyst. Nanoeng.*, 2024, **10**, 1.
36 J. Gao, *et al.*, Application of photocrosslinkable hydrogels based on photolithography 3D bioprinting technology in bone tissue engineering, *Regen. Biomater.*, 2023, **10**, rbad037.
37 B. Grigoryan, *et al.*, Multivascular networks and functional intravascular topologies within biocompatible hydrogels, *Science*, 2019, **364**, 458–464.
38 P. Kunwar, *et al.*, Printing Double-Network Tough Hydrogels Using Temperature-Controlled Projection Stereolithography (TOPS), *ACS Appl. Mater. Interfaces*, 2023, **15**, 30780–30792.
39 J. J. S. Rickard, I. Farrer and P. Goldberg Oppenheimer, Tunable Nanopatterning of Conductive Polymers via Electrohydrodynamic Lithography, *ACS Nano*, 2016, **10**, 3865–3870.
40 R. K. Pal, A. A. Farghaly, M. M. Collinson, S. C. Kundu and V. K. Yadavalli, Photolithographic Micropatterning of Conducting Polymers on Flexible Silk Matrices, *Adv. Mater.*, 2016, **28**, 1406–1412.
41 S. Ouyang, *et al.*, Surface Patterning of PEDOT:PSS by Photolithography for Organic Electronic Devices, *J. Nanomater.*, 2015, **2015**, 1–9.
42 B. R. Simona, *et al.*, Density gradients at hydrogel interfaces for enhanced cell penetration, *Biomater. Sci.*, 2015, **3**, 586–591.
43 R. Moser, *et al.*, From Playroom to Lab: Tough Stretchable Electronics Analyzed with a Tabletop Tensile Tester Made from Toy-Bricks, *Adv. Sci.*, 2016, **3**, 1500396.
44 Zurich Zentralbibliothek. Historic Map of Cyprus.
45 NASA. Satellite view of Cyprus.
46 E. B. Malarkey, *et al.*, Conductive Single-Walled Carbon Nanotube Substrates Modulate Neuronal Growth, *Nano Lett.*, 2009, **9**, 264–268.
47 J. S. Goldner, J. M. Bruder, G. Li, D. Gazzola and D. Hoffman-Kim, Neurite bridging across micropatterned grooves, *Biomaterials*, 2006, **27**, 460–472.
48 J. A. Shepard, *et al.*, Hydrogel design for supporting neurite outgrowth and promoting gene delivery to maximize neurite extension, *Biotechnol. Bioeng.*, 2012, **109**, 830–839.
49 A. M. Siddiqui, *et al.*, Promoting Neuronal Outgrowth Using Ridged Scaffolds Coated with Extracellular Matrix Proteins, *Biomedicines*, 2021, **9**, 479.
50 H. Liu, *et al.*, Filamented Light (FLight) Biofabrication of Highly Aligned Tissue-Engineered Constructs, *Adv. Mater.*, 2022, **34**, e2204301.

